Signal-Based Dynamic Identification of Composite Steel–Concrete Bridges Using Short-Duration Records

infrastructures

MDPI

Article

Signal-Based Dynamic Identification of Composite Steel–Concrete Bridges Using Short-Duration Records

Mario Ferrara [1,*], Gabriele Bertagnoli [1], Alessandro Imperiale [1] and Davide Masera [2]

[1] Department of Structural, Geotechnical and Buildng Engineering (DISEG), Politecnico di Torino, Corso Duca degli Abruzzi, 24, 10129 Torino, Italy; gabriele.bertagnoli@polito.it (G.B.); alessandro.imperiale@polito.it (A.I.)
[2] Masera Engineering Group Srl, Corso Bolzano 14, 10121 Torino, Italy; davide.masera@masera-eg.com
* Correspondence: mario.ferrara@polito.it

Abstract

Structural Health Monitoring (SHM) of existing bridges increasingly relies on dynamic measurements to assess structural performance and detect potential damage. However, the practical implementation of long-term vibration-based monitoring is still constrained by the volume of data required and the complexity of continuous acquisition systems. In the context of ensuring the safety and performance of existing bridge infrastructure, vibration-based monitoring offers a powerful tool for detecting changes in structural behavior. This study presents an extended investigation of dynamic monitoring applied to composite steel–concrete viaducts, focusing particularly on the signal-analysis framework and methodological enhancements. Short-duration accelerometric records are processed through an automated signal-selection pipeline and advanced modal-parameter extraction algorithms to yield identification of modal features. Emphasis is placed on the statistical evaluation of modal-parameter stability, effects of operational and environmental variability, and the potential for long-term trend detection. The results highlight the limits of short-length recordings when OMA techniques are applied. Nevertheless, appropriate signal processing and data handling can provide acceptable insights into the dynamic characteristics of large bridge systems. The methodological findings provide a foundation for improved monitoring workflows, showing the amount of information that can be retrieved using a cost-effective hardware deployment and supporting further development toward structural digital twins.

Keywords: bridge dynamic identification; Operational Modal Analysis; structural health monitoring; composite bridge

Academic Editors: Alexandre A. Cury, Abdollah Malekjafarian, Alessandro Sabato and Flavio Barbosa

Received: 31 December 2025
Revised: 23 January 2026
Accepted: 29 January 2026
Published: 2 February 2026

1. Introduction

The structural safety and serviceability of existing bridges have become a critical concern in many industrialized countries, where a large portion of the infrastructure network was built between the 1950s and 1980s and has now reached or exceeded its original design life. Aging, material degradation, and increased traffic loads have emphasized the urgent need for reliable tools capable of assessing the structural performance of these systems and detecting early signs of deterioration [1].

Within this framework, Structural Health Monitoring (SHM) represents a key strategy for improving infrastructure management, offering the potential to transform traditional inspection-based approaches into continuous, data-driven procedures that support predictive maintenance and informed decision-making [2]. Among the various SHM techniques,

vibration-based monitoring and Operational Modal Analysis (OMA) have proven particularly effective for identifying the dynamic properties of bridges, such as natural frequencies, damping ratios, and mode shapes, under ambient excitation [3–5]. These parameters provide valuable insight into the global stiffness and integrity of bridge systems and serve as sensitive indicators of structural change.

Despite their advantages, the practical implementation of OMA-based monitoring in real bridge infrastructure remains limited due to challenges such as the large volume of acquired data, the complexity of continuous acquisition systems, and the computational effort required for long-term processing [5–8].

Long-term monitoring studies have shown that environmental and operational effects, including temperature variations and traffic conditions, can significantly influence the identified modal parameters, complicating their interpretation in terms of structural condition [9,10].

Recent advances in wireless sensing, low-cost accelerometers, and IoT-based platforms have enabled large-scale SHM deployments. However, the management and processing of massive datasets remain critical bottlenecks.

While sensors have become more accessible, the cost, maintenance, and data-handling requirements of continuous long-duration measurements are often unsustainable for existing bridges. As a result, increasing attention is being directed toward signal-efficient monitoring strategies that enable reliable modal identification using short-duration recordings and a limited number of sensors [11–14]. In this context, several authors have investigated automated and continuous OMA procedures aimed at reducing human intervention and improving scalability in long-term applications [15,16].

Previous research has explored techniques to optimize the trade-off between data length and identification accuracy, such as advanced signal processing, statistical filtering, and automated selection of high-quality accelerometric data [17–19]. Specific studies have addressed the influence of record length, excitation variability, and signal quality on the stability of OMA results, highlighting the limitations of short-duration measurements when applied without adequate selection and validation criteria [20,21]. However, the influence of short record duration, variable signal quality, and environmental fluctuations on the stability of modal parameters remains an open topic, particularly for composite steel–concrete bridges, where material heterogeneity and boundary complexity strongly affect the dynamic behavior [3,5].

This paper contributes to this ongoing discussion by providing a critical and realistic assessment of a signal-based dynamic identification framework applied to an existing set of composite steel–concrete bridges equipped with a minimal monitoring system. The dataset is characterized by short, intermittent acceleration records (102.4 s) acquired through a sparse network of wireless sensors, which represents a common but challenging configuration in real-world SHM applications. The objective is not to demonstrate high-end performance but to evaluate how much reliable information can be extracted from limited and imperfect data, and to define the boundaries of applicability of short-duration vibration-based monitoring.

The methodology integrates automated signal selection, OMA, and clustering for extracting modal parameters from short acceleration records. Two complementary approaches are investigated and compared: a three-set approach, in which three independent high-energy short datasets are analyzed separately; and a merged-signal approach, where the same recordings are concatenated to simulate longer acquisitions.

The originality of the proposed framework lies in the way energetic recordings are selected and synchronized across the monitoring system, rather than in the definition of new modal identification techniques. In particular, signal selection is based on the

combined use of multiple energy-related indicators and on their temporal recurrence, with the aim of identifying acquisition instants that are consistently informative across different criteria and sensors.

The proposed comparison allows for quantifying the effects of record length, excitation variability, and data-handling strategy on modal identification accuracy and stability. The analysis also explores the impact of environmental and operational conditions—such as traffic intensity and temperature—on modal visibility and parameter consistency.

Overall, the study demonstrates that, although the monitoring system and the acquired data are far from ideal, careful signal processing, energy-based selection, and statistical validation can still provide meaningful insights into the dynamic behavior of large bridge structures. The findings offer practical guidance for engineers working with limited monitoring systems, showing that, despite significant constraints, it is still possible—by fully exploiting the available information—to obtain a coarse but meaningful assessment of the structural behavior.

2. Case Study and Monitoring Setup Description

The proposed signal-based identification framework was implemented and tested on an existing composite steel–concrete bridge system forming part of a major highway interchange in Northern Italy. The structure represents a typical example of medium-span composite viaducts, characterized by repetitive span configurations and subjected to high levels of traffic-induced vibration.

2.1. Structural Configuration

The interchange is composed of six viaducts, identified by specific numerical codes and corresponding color labels shown in Figure 1, which presents the plan view of the entire interchange. These are structures 2A2 (green), 223 (red), 210 (yellow), 233 (blue), 2B4 (orange), and 243 (violet).

Figure 1. Interchange overview. The arrows indicate the traffic direction.

The monitored viaduct system consists of multiple simply supported spans with lengths ranging from 25 to 36 m. Each span is composed of a reinforced-concrete deck slab supported by either two longitudinal steel girders (i.e., viaducts 210, 2B4, 2A2, and 243) or four longitudinal steel girders (i.e., viaducts 223 and 233), as shown in Figure 2. These girders are connected through transverse beams to ensure transversal distribution of the vehicular loads. The superstructure rests on circular reinforced-concrete piers based on shallow foundations.

(**a**) (**b**)

Figure 2. Example of 4-beam viaduct (**a**) and 2-beam viaduct (**b**).

The support system adopted at the piers, shown in Figure 3, represents one of the most distinctive features of this bridge type. In each pier region, one span rests directly on the columns, transferring loads through conventional steel bearings, while the adjacent span is suspended from the first one through a hanging-link system. As a result, each deck is alternately supported and suspended: at one end it sits directly on the pier, whereas at the opposite end it is hung from the neighboring span. This configuration produces a coupled dynamic interaction between consecutive spans, modifying both the effective boundary conditions and the modal characteristics of the decks. Although this arrangement efficiently accommodates longitudinal displacements, it also introduces additional complexity in interpreting the measured dynamic response as the stiffness of the hanger in the horizontal transverse direction is quite uncertain.

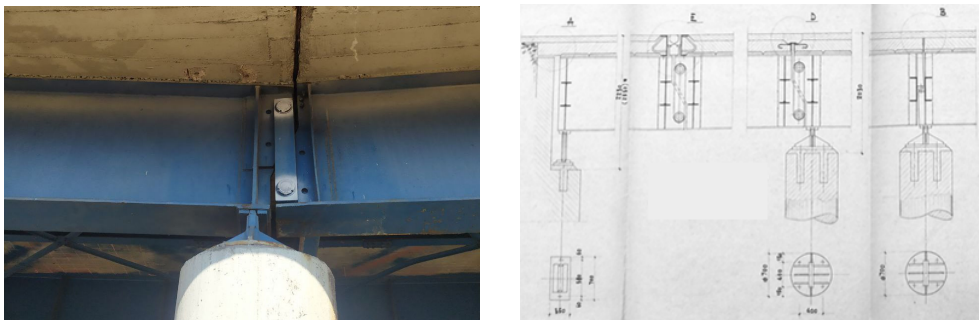

Figure 3. Detail of the 'Gerber' pendulum support system on the piers.

2.2. Monitoring Instrumentation

The monitoring system installed on the bridge includes both dynamic and static sensors, designed to capture complementary aspects of structural behavior. Static instrumentation comprises inclinometers and strain gauges, which are used to monitor slow-varying phenomena such as deflection trends, long-term deformations, and stress variations in critical sections.

In several viaducts, the monitoring system is installed on two contiguous spans, allowing for the evaluation of coupled responses of adjacent decks. The measurement layout adopted for this configuration is illustrated for a two-girder deck in Figure 4 and for a four-girder deck in Figure 5.

The present study focuses exclusively on the dynamic components of the monitoring system, which consist of a network of triaxial wireless accelerometers. These are composed of compact, battery-powered triaxial sensors. Each unit is capable of measuring acceleration along the longitudinal, transverse, and vertical axes, with a sampling frequency of 80 Hz. The sensors communicate with a central gateway unit via a low-power wireless protocol, enabling remote data acquisition and configuration without physical wiring.

This configuration drastically reduces installation time and maintenance requirements, making it particularly suited for medium-to-long-term monitoring campaigns on opera-

tional bridges. Each device includes an internal data buffer, temperature compensation, and clock synchronization routines to ensure temporal alignment among sensors.

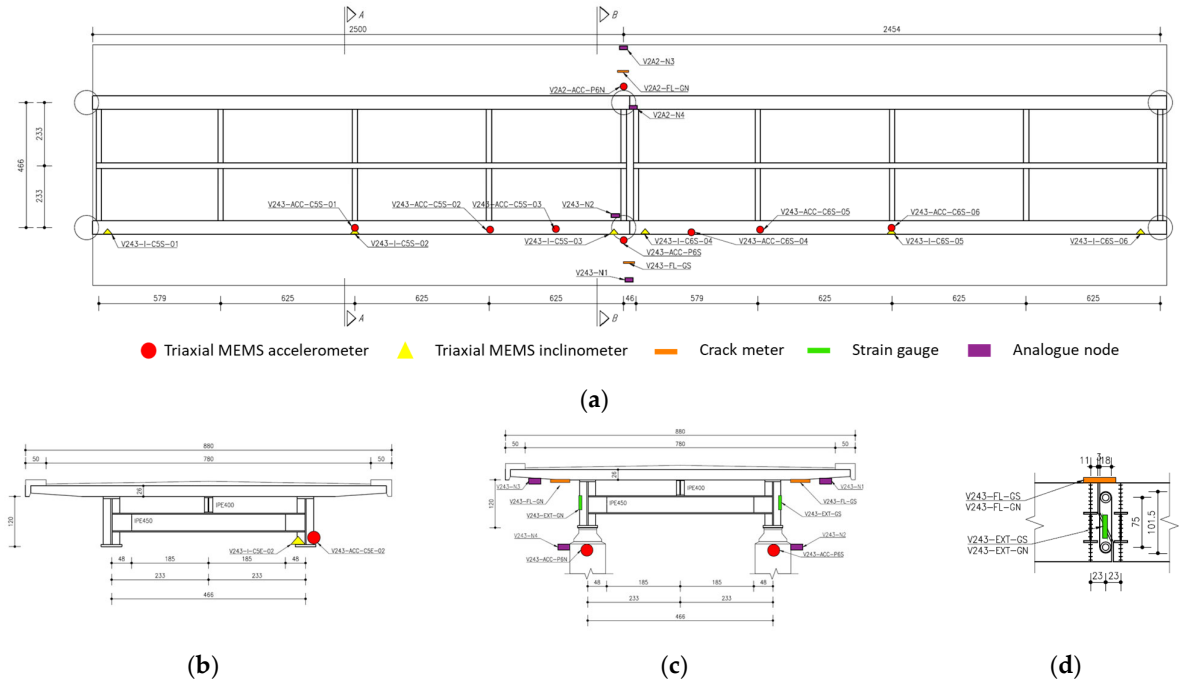

Figure 4. Typical arrangement of monitoring instruments on a double-girder viaduct. (**a**) Plan view. (**b**) Section at the mid-span of the deck. (**c**) Section on the piers. (**d**) Detail of the bearing.

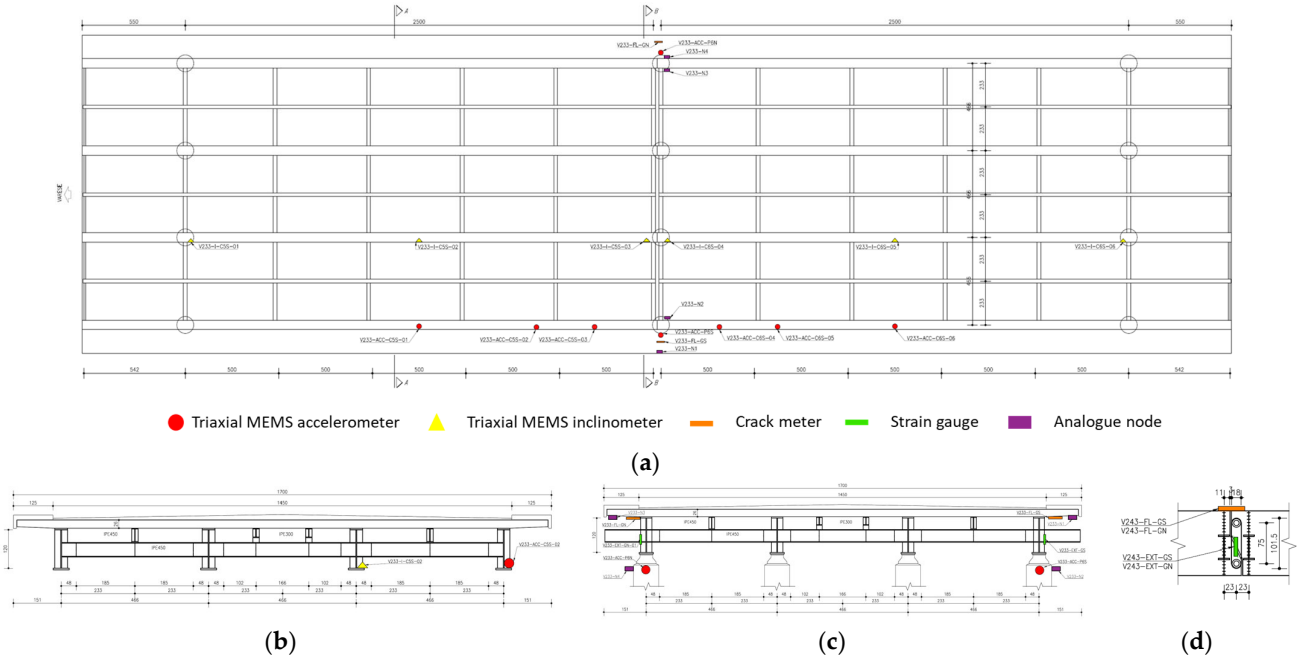

Figure 5. Typical arrangement of monitoring instruments on a four-girder viaduct. (**a**) Plan view. (**b**) Section at the mid-span of the deck. (**c**) Section on the piers. (**d**) Detail of the bearing.

The sensors were installed at a limited number of representative locations along selected spans:

- Mid-span (L/2), capturing the maximum vertical displacements;
- Quarter-span (L/4) and one-eighth span (L/8), corresponding to regions of high modal curvature;

- Pier tops, where acceleration levels are expected to be lower but phase information is valuable for mode-shape identification.

The combination of these positions provides a minimal yet informative measurement layout, allowing evaluation of how a reduced number of sensors affects the accuracy of modal identification.

2.3. Data Acquisition Strategy

The accelerometers can acquire only short-duration acceleration records. Their use in Operational Modal Analysis (OMA) and in the evaluation of vibration-based indicators of structural performance is assessed in the paper.

Two complementary data acquisition modes were configured:

- Scheduled acquisitions, automatically performed at fixed time intervals (e.g., every 6 h from January 2023 to December 2023), each lasting 102.4 s—equivalent to 8192 samples per channel (the maximum length permitted by the memory of the sensor). These measurements were primarily used for Operational Modal Analysis (OMA).
- Triggered acquisitions, activated when the measured acceleration exceeds a predefined threshold. Each triggered record lasts 12.8 s (1024 samples) and captures short-duration, high-intensity events such as the passage of heavy vehicles.

3. Motivation for the Proposed Signal-Based Strategy

During the preliminary phase of the study, it became evident that the direct application of OMA techniques to all available acceleration records was neither practical nor useful. Two main factors motivated the development of a signal-based procedure driven by the energy content of the recordings: computational limitations and variability of identification results.

The monitoring system produces a large number of scheduled acquisitions, one every six hours, resulting in thousands of short acceleration records per year.

Performing a complete OMA on every single scheduled acquisition would require substantial computational time and memory, as it is repeated for multiple viaducts.

Preliminary analyses also revealed a high temporal variability in the modal parameters identified from each scheduled acquisition.

Each 102.4 s record captures the bridge response under specific and transient excitation conditions—mainly affected by traffic intensity, but also by temperature, wind, or humidity. Therefore, the number and stability of the identified modes vary considerably between consecutive acquisitions.

Some recordings yield clear stabilization diagrams with multiple consistent modes, while others produce only one or two weakly defined modes.

Figure 6 shows a collection of stabilization diagrams obtained over seven consecutive days of monitoring (i.e., from Sunday 1 January 2023 to Saturday 7 January 2023). Each row corresponds to one calendar day, while each column represents one of the four scheduled acquisitions: at 01:00, 07:00, 13:00, and 19:00 h. The frequency range investigated is 0–5 Hz.

In each diagram, blue dots denote poles stable in frequency, damping, and mode shape; green points indicate poles stable in frequency and damping only; and red points correspond to unstable poles.

A clear variability is observed among the four daily scheduled acquisitions and between consecutive days. Some time slots (for instance, daytime acquisitions around 07:00 and 13:00) show denser clusters of blue poles, indicating stronger excitation and better modal visibility—likely due to heavier traffic levels and thus higher vibration energy. In contrast, nighttime acquisitions (01:00) or those performed during calm environmental conditions often show sparser stabilization diagrams, with only a few stable.

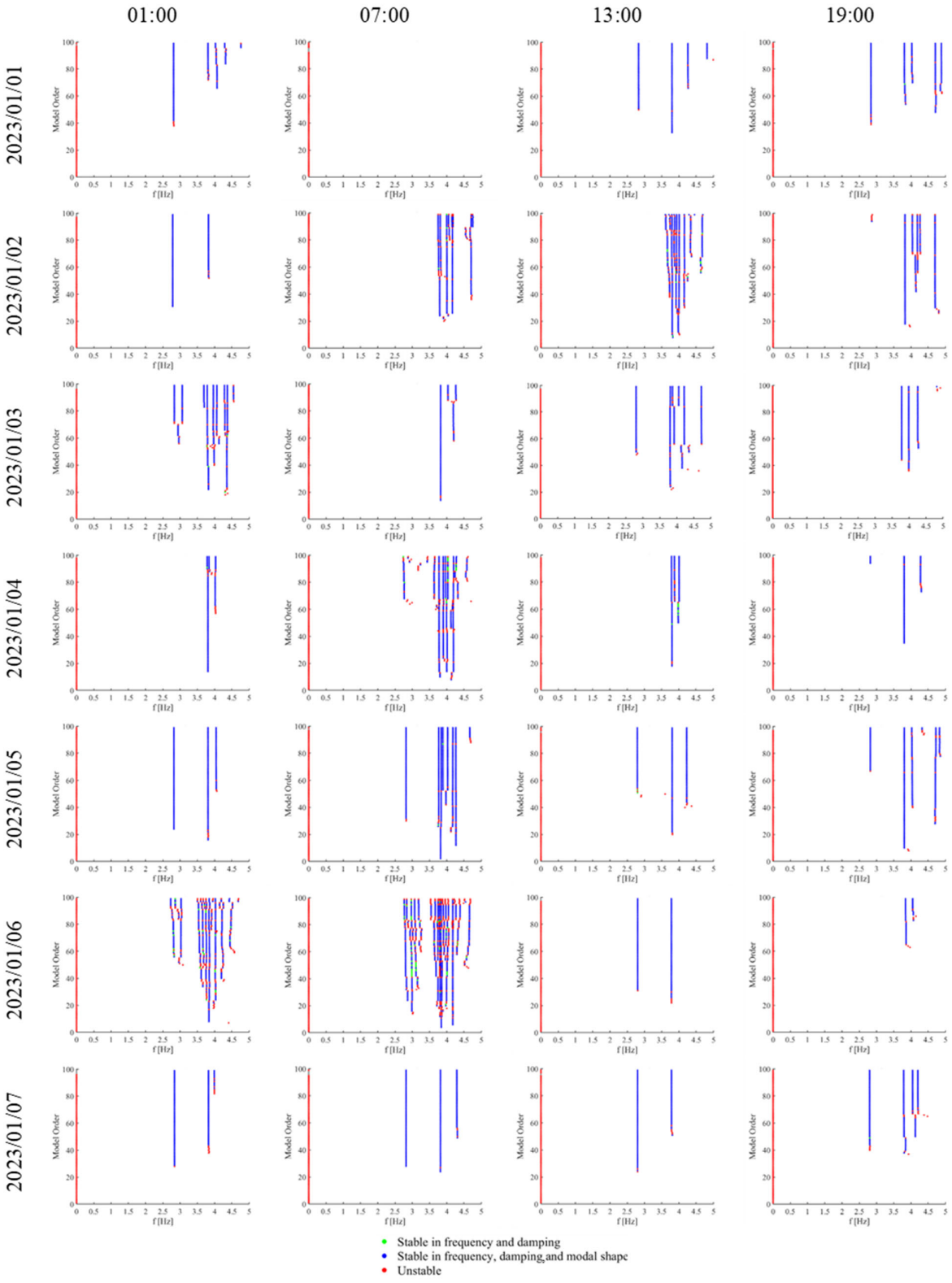

Figure 6. Stabilization diagrams obtained from scheduled acquisition from 1 January 2023 to 7 January 2023.

This pattern confirms that the modal visibility under ambient excitation depends strongly on both the energy level and spectral content of the input and on environmental and operational factors such as traffic, temperature, or wind [22,23].

In several cases, the same vibration modes appear intermittently—well defined in some diagrams and barely visible in others—demonstrating the high temporal variability that characterizes non-controlled ambient-vibration tests.

Figure 7 shows all the natural frequencies identified during January 2023 from the complete set of scheduled acquisitions for viaduct 2A2.

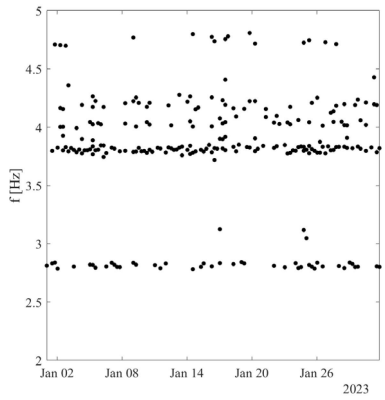

Figure 7. Natural frequencies identified from all scheduled acquisitions during January 2023 for viaduct 2A2.

The plot highlights the large dispersion of results obtained when every available signal is processed without any selection. Although several clusters of recurring frequencies can be recognized—approximately around 2.8 Hz, 3.75 Hz, 4.0 Hz, and 4.2 Hz, corresponding to the bridge's main vibration modes—the number and clarity of the identified modes vary considerably.

This variability reflects the influence of excitation level and environmental conditions on the visibility of modes under ambient vibrations: some records, typically characterized by higher energy, provide well-defined modes, while others yield only partial or noisy identifications. The figure therefore illustrates the need for a selective processing strategy.

Such variability justifies the need for the energy-driven signal-selection procedure adopted in this study. By identifying and analyzing only the most energetic recordings, the methodology minimizes the inclusion of low-excitation or noisy signals, thus improving the reliability and consistency of the OMA results while drastically reducing computational demand.

Consequently, a selective approach was required to identify and process only those recordings containing sufficient dynamic energy to ensure robust and repeatable identification.

The adopted strategy—described in detail in the following section—therefore aims to balance computational efficiency and modal reliability by automatically selecting a limited number of high-energy, high-quality signals.

This approach drastically reduces processing effort while preserving the physical representativeness of the dataset, enabling effective modal identification even within a large, heterogeneous set of short acceleration records.

4. Methodology and Results

The methodological framework adopted in this study aims to extract reliable dynamic characteristics (i.e., frequencies and modal shapes) of composite bridge decks from short-duration acceleration records (102.4 s), while minimizing manual intervention in data processing. The complete workflow consists of four main stages:

1. Preprocessing and signal conditioning,
2. Automated signal selection,
3. Modal-parameter identification,

4. Statistical evaluation and validation.

A schematic representation of the process is provided in Figure 8.

Figure 8. Schematic representation of the workflow.

In parallel, a complementary analysis was performed on the short triggered accelerograms (12.8 s), automatically recorded when acceleration thresholds were exceeded. These data were processed to evaluate the peak dynamic response and its long-term evolution, providing additional insights that support the interpretation of the modal identification results discussed in Section 4.6.

4.1. Data Preprocessing and Conditioning

All acceleration records collected from the monitoring system are first subjected to a standardized preprocessing routine, developed in MATLAB version 2023b [24], to ensure consistency and comparability. Each raw signal is filtered using a band-pass filter tailored to the expected frequency range of the bridge (0–20 Hz) [3,14], as shown in Figure 9. Signals affected by data gaps or excessive noise are also automatically excluded through quality-control metrics.

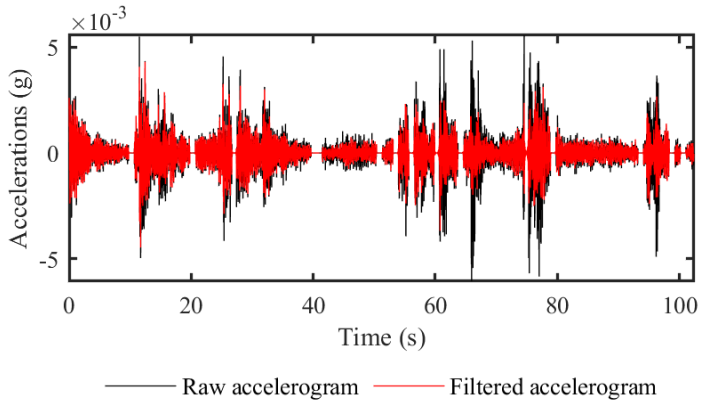

Figure 9. Example of raw and filtered accelerations.

4.2. Automated Signal Selection

A signal-selection algorithm was developed in MATLAB [18] to automatically identify, for each month, the accelerograms with the highest energy and modal content.

For every triaxial sensor, three energy-based indicators were computed from each 102.4 s acquisition:

1. The standard deviation of the acceleration time history;
2. The area under the Power Spectral Density (PSD) curve in the frequency ranges under investigation (0 to 20 Hz), as shown in Figure 10a;
3. The maximum peak of the PSD function in the frequency ranges under investigation (0 to 20 Hz), as shown in Figure 10b.

Figure 10 reports an example of the second and third energy-based method applied to four randomly selected acquisitions in January 2023 for viaduct 2A2 to illustrate the criteria adopted for the automatic signal selection. The first plot (Figure 10a) refers to the area-based approach, in which the total energy content of the Power Spectral Density (PSD) curve is integrated over the frequency range of interest. The second plot (Figure 10b)

corresponds to the maximum-peak approach, where the signal is ranked according to the highest amplitude observed in the PSD.

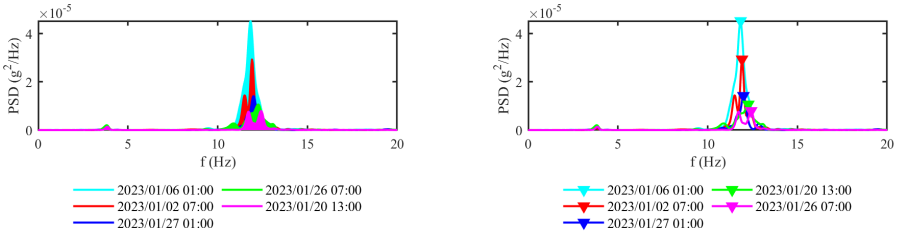

(**a**) (**b**)

Figure 10. Example of signal selection based on energy content. (**a**) Method based on the maximum area under the PSD. (**b**) Method based on the maximum peak of the PSD.

Table 1 reports the numerical results for the same four dates. As can be seen from the comparison, the three methods generally identify the same recordings as the most energetic. In many cases, but not always, the recordings with the largest integrated PSD area coincide with the ones showing the highest spectral peak and the highest standard deviation, confirming the consistency between the three selection criteria. Nevertheless, it is possible, like in the example proposed in Figure 10 and in Table 1, that the different criteria provide different results when asked to select the most energetic accelerogram. In this case 1 January 2023 h07:00 is the best sample of January in terms of standard deviation but the second-best for PSD area and peak, whereas 20 January 2023 h13:00 ranks first according to the area and peak but second for standard deviation. The third-best is unanimously 6 January 2023 h01:00.

Table 1. Example of signal selection based on energy content for four random dates in January 2023 for viaduct 2A2.

Date	Standard Deviation	PSD Area	PSD Peak
1 January 2023 07:00	5.80×10^{-3} (1st)	1.90×10^{-5} (2nd)	2.94×10^{-5} (2nd)
6 January 2023 01:00	3.50×10^{-3} (3rd)	1.05×10^{-5} (3rd)	1.42×10^{-5} (3rd)
20 January 2023 13:00	5.40×10^{-3} (2nd)	3.46×10^{-5} (1st)	4.52×10^{-5} (1st)
26 January 2023 07:00	2.80×10^{-3} (5th)	7.53×10^{-6} (4th)	7.96×10^{-6} (5th)
27 January 2023 01:00	3.40×10^{-3} (4th)	1.33×10^{-6} (5th)	1.07×10^{-5} (4th)

To ensure temporal consistency among sensors, the selected acquisitions were further screened based on their recurrence in time.

For each sensor installed on a given structure, and for each selection metric (i.e., maximum standard deviation, maximum PSD peak, and maximum PSD area), the dates of the three most energetic records were extracted on a monthly basis. An example of the resulting candidates is reported in Table 2.

Table 2. Viaduct 2A2, January 2023. Monthly selection of the three most energetic accelerometric records for each sensor and selection criterion.

		Vertical direction			
		Pier	L/8	L/4	L/2
Standard Deviation	1st	2023-01-31_07-00	2023-01-02_07-00	2023-01-27_01-00	2023-01-27_01-00
	2nd	2023-01-13_13-00	2023-01-27_01-00	2023-01-06_01-00	2023-01-06_01-00
	3rd	2023-01-19_13-00	2023-01-06_01-00	2023-01-02_07-00	2023-01-02_07-00

Table 2. *Cont.*

		Vertical direction			
PSD Peak	1st	2023-01-17_07-00	2023-01-27_01-00	2023-01-27_01-00	2023-01-27_01-00
	2nd	2023-01-19_13-00	2023-01-06_01-00	2023-01-06_01-00	2023-01-06_01-00
	3rd	2023-01-31_07-00	2023-01-26_07-00	2023-01-10_13-00	2023-01-10_13-00
PSD Area	1st	2023-01-31_07-00	2023-01-27_01-00	2023-01-27_01-00	2023-01-27_01-00
	2nd	2023-01-13_13-00	2023-01-20_13-00	2023-01-06_01-00	2023-01-06_01-00
	3rd	2023-01-19_13-00	2023-01-02_07-00	2023-01-31_07-00	2023-01-31_07-00
		Longitudinal direction			
		Pier	L/8	L/4	L/2
Standard Deviation	1st	2023-01-17_07-00	2023-01-31_07-00	2023-01-26_07-00	2023-01-26_07-00
	2nd	2023-01-26_07-00	2023-01-26_07-00	2023-01-17_07-00	2023-01-17_07-00
	3rd	2023-01-31_07-00	2023-01-17_07-00	2023-01-19_13-00	2023-01-19_13-00
PSD Peak	1st	2023-01-17_07-00	2023-01-17_07-00	2023-01-26_07-00	2023-01-26_07-00
	2nd	2023-01-31_07-00	2023-01-26_07-00	2023-01-17_07-00	2023-01-19_13-00
	3rd	2023-01-26_07-00	2023-01-19_13-00	2023-01-19_13-00	2023-01-17_07-00
PSD Area	1st	2023-01-17_07-00	2023-01-31_07-00	2023-01-17_07-00	2023-01-26_07-00
	2nd	2023-01-26_07-00	2023-01-26_07-00	2023-01-26_07-00	2023-01-17_07-00
	3rd	2023-01-31_07-00	2023-01-17_07-00	2023-01-19_13-00	2023-01-19_13-00
		Transverse direction			
		Pier	L/8	L/4	L/2
Standard Deviation	1st	2023-01-31_07-00	2023-01-19_13-00	2023-01-19_13-00	2023-01-19_13-00
	2nd	2023-01-19_13-00	2023-01-26_07-00	2023-01-31_07-00	2023-01-31_07-00
	3rd	2023-01-23_13-00	2023-01-31_07-00	2023-01-20_13-00	2023-01-20_13-00
PSD Peak	1st	2023-01-31_07-00	2023-01-19_13-00	2023-01-19_13-00	2023-01-19_13-00
	2nd	2023-01-19_13-00	2023-01-31_07-00	2023-01-14_13-00	2023-01-31_07-00
	3rd	2023-01-14_13-00	2023-01-14_13-00	2023-01-31_07-00	2023-01-14_13-00
PSD Area	1st	2023-01-31_07-00	2023-01-19_13-00	2023-01-19_13-00	2023-01-19_13-00
	2nd	2023-01-19_13-00	2023-01-26_07-00	2023-01-31_07-00	2023-01-31_07-00
	3rd	2023-01-26_07-00	2023-01-31_07-00	2023-01-20_13-00	2023-01-20_13-00

Based on the acquisition dates identified in Table 2, a recurrence analysis was then performed by counting how often each date appears across the different sensors and selection criteria. This procedure allows the identification of the acquisition instants shared by the largest number of sensors.

Complete simultaneity of peak energy values across all sensors is not required, as it is rarely achieved in operational monitoring conditions. Instead, the selection process aims to identify the time windows with the largest number of high-energy synchronous recordings available for each viaduct.

Using a single energy metric, i.e., PSD peak, PSD area, or signal standard deviation, generally leads to results similar to the ones obtained combining the three approaches, but sometimes one single metric identifies accelerograms that are not the most energetic. In particular, the max PSD peak misleads the selection in roughly 8% of cases, whereas PSD area and standard deviation generally agree. The advantage of the proposed multi-metric framework is the increase in the robustness of the procedure by reducing the dependence on a single indicator and mitigating possible discrepancies or errors.

The resulting recurrence counts, which quantify the level of temporal synchronization among sensors, are reported in Table 3.

At the end of the selection process, three datasets were defined for each month (the first and second time windows count 22 out of the 36 most energetic occurrences, whereas the third only counts 16 out of 36). The time window with the highest recurrence was assigned to Set 1, the second most recurrent date to Set 2, and the third most recurrent

date to Set 3. These three datasets were then used for the subsequent Operational Modal Analysis (OMA).

Table 3. Viaduct 2A2, January 2023. Recurrence analysis of acquisition dates across sensors and selection criteria. Green first set, blue second set, yellow third set.

Vertical Direction				Longitudinal Direction				Transverse Direction			
Pier	**L/8**	**L/4**	**L/2**	**Pier**	**L/8**	**L/4**	**L/2**	**Pier**	**L/8**	**L/4**	**L/2**
22	4	9	9	13	22	16	16	22	22	22	22
2	9	8	8	16	16	13	13	22	16	22	22
22	8	4	4	22	13	22	22	1	22	5	5
13	9	9	9	13	13	16	16	22	22	22	22
22	8	8	8	22	16	13	22	22	22	4	22
22	16	2	2	16	22	22	13	4	4	22	4
22	9	9	9	13	22	13	16	22	22	22	22
2	5	8	8	16	16	16	13	22	16	22	22
22	4	22	22	22	13	22	22	16	22	5	5

This approach allows the analysis to exploit the maximum possible spatial information while preserving temporal consistency among sensors. The synchronization and selection procedure was performed individually for each viaduct, ensuring that each dataset used for OMA represents the most complete and temporally consistent configuration of the available measurements.

Although in this study the selection was carried out on a monthly basis, the procedure is fully scalable in time and can be applied over different aggregation intervals—such as weekly or quarterly windows—depending on signal quality, monitoring objectives, and the desired temporal resolution of the analysis.

The proposed selection algorithm ensures that only high-quality signals with sufficient excitation energy are processed, drastically reducing computational demand while preserving the representativeness of the dataset. It also enables consistent temporal sampling of the structure's dynamic behavior, facilitating long-term monitoring and statistical trend analysis.

4.3. Operational Modal Analysis (OMA)

Modal identification is carried out using the Covariance-driven Stochastic Subspace Identification—(SSI-Cov) algorithm [3,25], implemented in MATLAB [24].

In SSI-based identification, two parameters strongly affect the accuracy, robustness, and computational cost of the analysis: the model order, which defines the dimension of the state-space system to be identified, and the number of block rows, which determines the size of the block Toeplitz (or Hankel) matrices used to project the system dynamics in the subspace domain [26].

If the model order is set too low, physical modes may merge or be partially represented, producing biased estimates and spurious damping values. Conversely, an excessively high model order introduces a large number of mathematical (noise-related) modes, complicating the stabilization diagram and significantly increasing computation time and memory usage [26].

Similarly, the number of block rows influences the conditioning of the identification matrices: a small number leads to ill-conditioned systems and poor separation between signal and noise, while an excessive number increases numerical instability and computational demand without improving accuracy [26].

According to the sensitivity analyses and recommendations of [26], reliable and stable results for civil structures are typically obtained when the maximum model order is conservatively chosen between 60 and 100 and the number of block rows is selected so as to ensure adequate over-specification of the system while keeping the inversion problem well posed. Increasing either parameter enhances stabilization up to a point, beyond which spurious modes begin to appear and the benefit on modal accuracy diminishes.

Based on preliminary calibration analyses performed on the present dataset, and following the guidance above, the maximum model order was set to 100. This value represents a practical balance between accuracy and computational efficiency, ensuring that all relevant vibration modes are captured without excessive redundancy. The number of block rows i was set as a function of the maximum model order $n_{\max}$ and the number of measured outputs m, enforcing $im \geq 2n_{\max}$ (i.e., $i = \lceil 2n_{\max}/m \rceil$) to ensure a sufficiently tall extended observability matrix and reduce ill-conditioning of covariance/Hankel matrices [26].

For each structure, stabilization diagrams were generated for the three data sets (Set 1, Set 2, and Set 3) of each month. The stable poles were identified as those fulfilling the stabilization conditions defined by Equation (1), which simultaneously evaluate the convergence of frequency, damping ratio, and mode-shape correlation across increasing model orders.

$$\frac{|f(n) - f(n+1)|}{f(n)} < 0.01 \tag{1a}$$

$$\frac{|\zeta(n) - \zeta(n+1)|}{\zeta(n)} < 0.05 \tag{1b}$$

$$1 - MAC(\{\Phi(n)\}, \{\Phi(n+1)\}) < 0.02 \tag{1c}$$

where n indicates the model order. MAC measures the similarity between two modal shapes. It varies between 0 and 1; 0 represents no correspondence between modal shapes, while 1 represents maximum correspondence between modal shapes. The MAC between two modal shapes, in the most general case of complex-valued vectors, is calculated as follows:

$$MAC(\{\Phi_1\}, \{\Phi_2\}) = \frac{|\{\Phi_1\}^H \cdot \{\Phi_2\}|^2}{\left(\{\Phi_1\}^H \cdot \{\Phi_1\}\right) \cdot \left(\{\Phi_2\}^H \cdot \{\Phi_2\}\right)} \tag{2}$$

The OMA procedures adopted yield complex eigenvalues and complex mode shapes. A distinction must therefore be made between normal (real) modes, characterized by in-phase motion of all Degrees of Freedom (DOFs), and complex modes, where phase differences occur among DOFs. In normal modes, all points reach their maximum and equilibrium positions simultaneously, whereas in complex modes these instants differ across the structure [3,27,28].

Complex modes may arise from non-proportional damping, nonlinearities, or physical coupling effects, but they can also result from measurement noise and limited signal quality. In practical applications, complex mode shapes are usually converted into real-valued vectors by adjusting the phase of each component to either 0° or 180°, ensuring a consistent and physically interpretable representation of the structural vibration patterns [27,28].

Figure 11 presents the stabilization diagrams obtained for Set 1, Set 2, and Set 3, corresponding to the three groups of synchronous accelerometric recordings selected for January 2023 for viaduct 2A2. Each diagram shows the poles identified by the SSI-Cov algorithm as a function of natural frequency and model order. The color coding differentiates between unstable poles (red), poles stable in frequency and damping (green), and poles stable also in modal shape (blue).

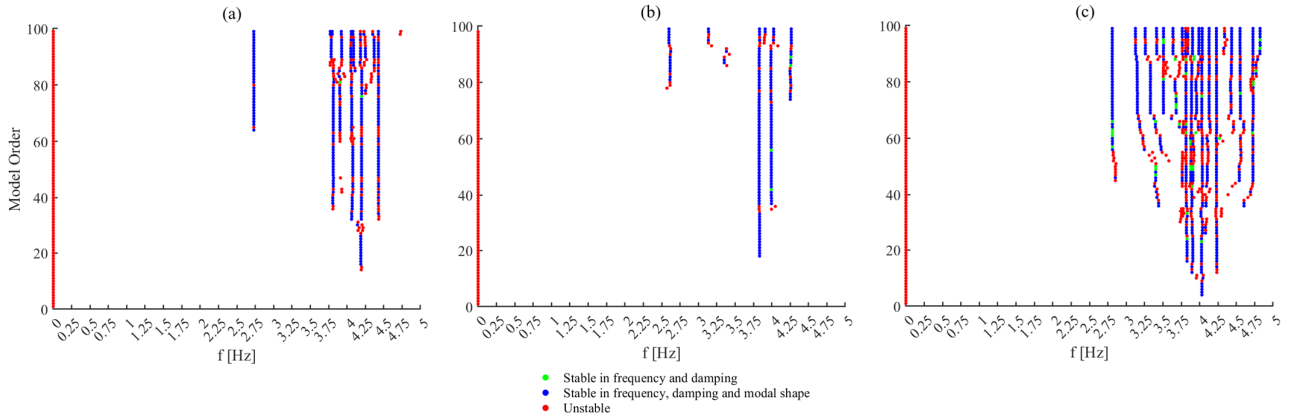

Figure 11. Example of stabilization diagrams obtained for January 2023 for viaduct 2A2. (**a**) Results for Set 1. (**b**) Results for Set 2. (**c**) Results for Set 3.

Across the three datasets, a consistent pattern of stable poles is observed, confirming the repeatability of the identified dynamic characteristics. The most pronounced vertical alignments of blue markers, corresponding to stable poles in all parameters, occur in the frequency range between 3 Hz and 5 Hz, which represents the dominant vibration region of the structure. Compared to Figure 6 (i.e., same structure and same month), it is possible to note a stable presence of certain alignments (i.e., 3.75 Hz, 4 Hz, and 4.2 Hz).

Figure 12 shows the stabilization diagram obtained from an artificial dataset, obtained by merging the accelerograms of Set 1, Set 2, and Set 3 one after the other for each sensor. A comparison with the stabilization diagrams shown in Figure 11 is discussed. The purpose of this comparison is to assess whether an artificial increase in signal duration, obtained by gluing nonconsecutive shorter acquisitions, improves the quality and clarity of modal identification.

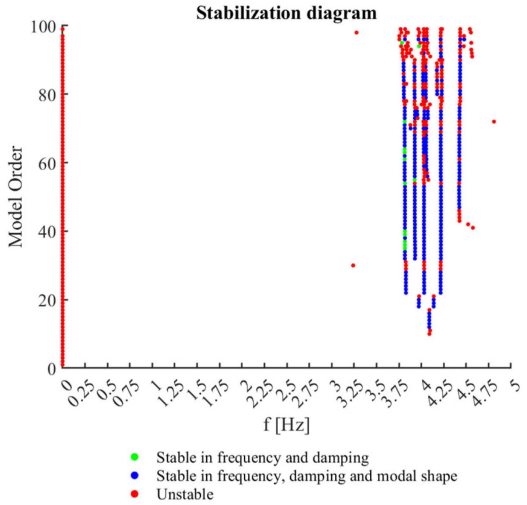

Figure 12. Example of stabilization diagrams obtained for January 2023 for viaduct 2A2 from the combination of the three datasets.

The combined dataset shows a stabilization pattern broadly consistent with those obtained from the individual sets. The same dominant modes appear clearly around 3–5 Hz. However, the extended signal length does not result in a significant enhancement of the stabilization diagram: the distribution of stable poles remains comparable to that of Set 1.

On the contrary, the artificial concatenation of signals slightly increases the number of spurious poles and local numerical instabilities, likely due to discontinuities and differences in excitation characteristics between recordings.

Overall, the results suggest that merging multiple short-duration recordings provides limited benefits in terms of modal clarity while introducing potential inconsistencies related to excitation variability and noise heterogeneity.

4.4. Clustering Process

The automatic identification of stable poles in stabilization diagrams has been extensively investigated in recent years and is widely discussed in the literature on Operational Modal Analysis. Several algorithms have been proposed to improve the objectivity and repeatability of modal-parameter extraction, reducing the dependence on user interpretation and enhancing the robustness of long-term monitoring applications [29–33].

The DBSCAN (Density-Based Spatial Clustering of Applications with Noise) algorithm [34] is applied in the frequency–damping space [33] to automate the detection of consistent poles. Clusters of stable poles represent the identified natural modes of the structure. In this study, the clustering parameters were defined to ensure both statistical robustness and selectivity: the minimum number of poles required to form a valid cluster was set equal to 50% of the maximum model order, while the maximum Euclidean distance between each pole and the cluster centroid was limited to 0.01; this value was determined through a sensitivity-based tuning process, seeking an optimal balance between cluster compactness and robustness of the modal identification results. These thresholds were chosen to guarantee the physical consistency of the identified modes and to filter out spurious poles associated with noise or weak stabilization.

Figure 13 illustrates an example of the clustering procedure applied to the stable poles identified through the SSI-Cov analysis.

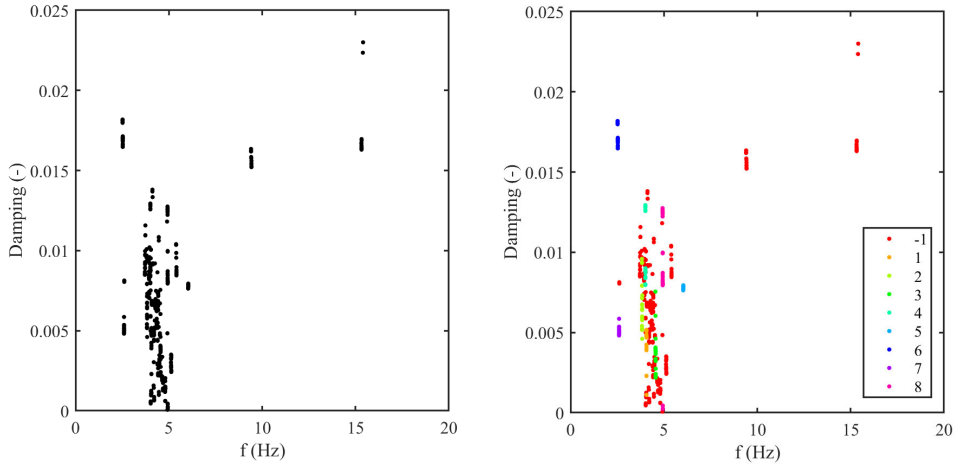

Figure 13. Example of application of the clustering algorithm for January 2023 for viaduct 2A2. (**a**) Plot of stable poles in the damping frequency space. (**b**) Clustering result.

Figure 13a shows the distribution of all stable poles in the frequency–damping space, obtained after the application of the stabilization criteria defined in Equation (1). Each point corresponds to a pole that remained stable across consecutive model orders.

Figure 13b presents the result of the DBSCAN clustering algorithm, used to automatically group poles associated with the same vibration mode.

In the figure, each color corresponds to a distinct cluster, while the label—1 identifies poles that do not belong to any cluster and are thus considered isolated or noise-related.

This automated clustering procedure allows for the objective identification of consistent modal frequencies and damping ratios, filtering out spurious poles and ensuring that each detected cluster represents a physically meaningful structural mode.

Once stable clusters are established for each month, their centroids are computed to determine the mean modal frequencies and damping ratios, while the corresponding mode shapes are reconstructed from the identified state-space matrices.

4.5. Estimation of Modal Parameters

The modes identified according to the procedure described in Section 4.3 were aggregated on an annual basis for each monitored viaduct. This resulted in a comprehensive dataset including all the modes identified throughout the year.

On this annual dataset, the identification of the structure's fundamental modes was carried out through a DBSCAN clustering algorithm [34]. The DBSCAN clustering was applied in the frequency–MAC space, where each identified mode is represented by its natural frequency and by the Modal Assurance Criterion (MAC) values computed with respect to all other modes identified during the same year.

Figure 14 illustrates an example of the DBSCAN clustering process applied to the annual dataset of identified modes.

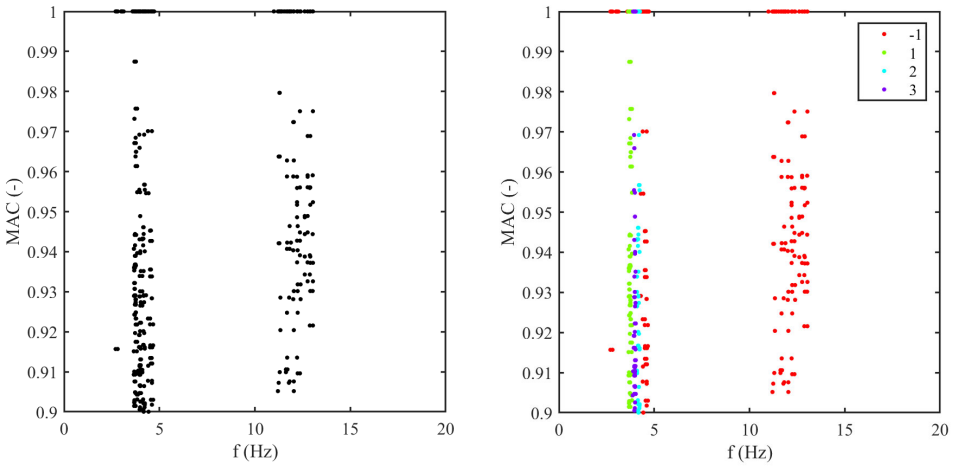

Figure 14. Example of application of the clustering algorithm for identifying recurring modes. (**a**) Plot of modes in the MAC frequency space. (**b**) Clustering result.

Figure 14a represents the distribution of all modes in the frequency–MAC space, where each point corresponds to a mode identified during the year. The Modal Assurance Criterion (MAC) quantifies the correlation between each mode and the other identified modes, allowing the assessment of their similarity in modal shape. Only modes with MAC values greater than 0.9 are displayed, as this threshold was adopted as the lower limit to ensure the inclusion of only highly correlated and physically meaningful modes. All modes with MAC < 0.9 were excluded from further analysis to prevent the influence of poorly correlated or spurious shapes.

Figure 14b shows the results of the clustering algorithm, where each color represents a distinct cluster corresponding to a recurring mode of the structure. The label—1 identifies isolated points that do not belong to any cluster. In the clustering configuration, the maximum Euclidean distance of each mode from the cluster centroid was set to 0.075, ensuring a compact grouping of modes with similar frequencies and modal shapes. The clustering distance parameter was selected through a sensitivity analysis of the clustering procedure. Due to the presence of closely spaced modes with very similar mode shapes, the chosen value represents a compromise that allows nearby modes to be distinguished without merging them into the same cluster, while avoiding ambiguous or unstable clustering results.

This procedure effectively groups modes that exhibit both frequency and modal-shape consistency throughout the year, thereby enabling the identification of the structure's fundamental modal families.

Figure 15a shows the final outcome of the annual modal identification and clustering procedure. Each colored series corresponds to one of the modes identified through the DBSCAN analysis described.

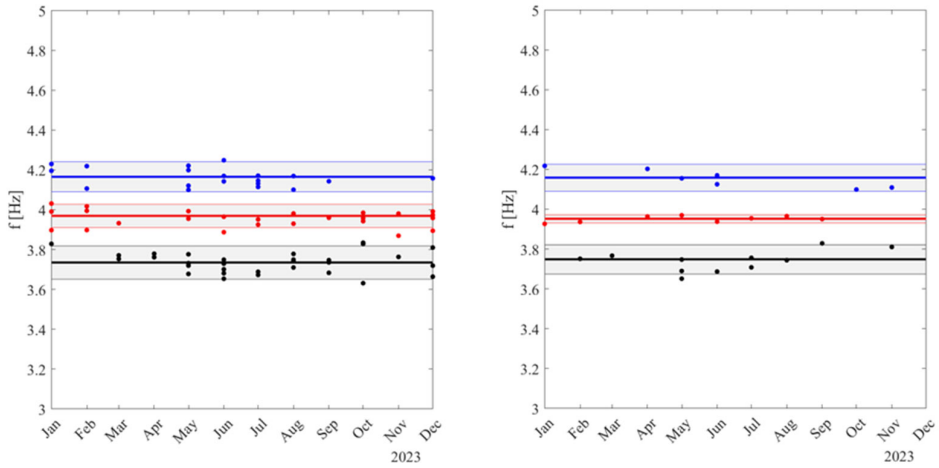

(**a**) (**b**)

Figure 15. Example of modes identified for viaduct 2A2 in the year 2023. (**a**) Results for analysis of the three selected sets of 102.4 s. (**b**) Results obtained by merging the three sets of 102.4 s. Black Mode 1, red Mode 2, and blue Mode 3.

For each mode, the thick central line represents the mean value of the natural frequency, while the shaded area of the same color indicates the confidence interval corresponding to the 5th and 95th percentiles of the normal distribution associated with that mode. The distribution of the identified modal frequencies was checked and was found to be approximately normal, with minor deviations at the tails. Therefore, non-parametric confidence intervals based on the 5th–95th percentiles were adopted to ensure robustness without relying on strict normality assumptions.

Figure 15b presents the results obtained by merging the three selected 102.4 s recordings for each month into a single dataset prior to modal identification. The results show frequency values and variability trends consistent with those obtained from the independent datasets. The confidence bands remain of similar width, and the number of identified modes is unchanged. In some cases, the artificial concatenation of short records may even introduce small inconsistencies due to non-stationary excitation conditions between different acquisitions.

Both methodologies (i.e., the three-set approach and the merged-signal approach) successfully identify the main modal alignments already visible in Figure 7, which reports the identification results for all scheduled recordings during January for viaduct 2A2. The frequencies obtained with both procedures are approximately 3.75 Hz, 3.95 Hz, and 4.20 Hz, matching the dominant clusters observed in the full-month analysis (shown in Figure 7).

However, one mode observed in Figure 7 at about 2.8 Hz is not captured by either of the two refined methodologies. This mode predominantly appears during nighttime or low-traffic conditions, when the excitation level is low and the vibration energy content is insufficient to activate the higher modes. In contrast, the high-energy records used in the present analysis correspond mainly to periods of intense traffic, in which that low-energy mode becomes less visible or completely suppressed.

Consequently, because the signal-selection strategy was driven by energy content, the methodology inherently filters out low-energy events, thereby improving the reliability of the dominant mode identification but losing information on the less-excited lower mode around 2.8 Hz.

In principle, the three-set approach should produce up to three modal estimates per month—one for each dataset—while the merged-signal approach should yield only one estimate. Nevertheless, in some months, four or five frequency values are observed in the first case and two or three in the second. This behavior can be attributed to several factors:

- The presence of closely spaced or interacting modes, which may occasionally be resolved as distinct clusters [35–37];
- Slight environmental or operational variations within the month (e.g., temperature changes or traffic-induced excitation differences) that cause small frequency shifts and lead the clustering algorithm to separate them into different modal groups [38];
- In the case of the merged dataset, non-stationary excitation introduced by concatenating signals from different recordings, which can generate duplicate poles around the same frequency band [39].

The mean frequency values and their temporal distribution obtained with the merged signals are very similar to those obtained with the three-set analysis, demonstrating that the artificial extension of record length does not lead to a substantial improvement in frequency stability or accuracy.

Table 4 reports the mean natural frequencies identified for each monitored viaduct, together with the corresponding standard deviation and coefficient of variation (CoV) computed over the annual dataset of short-duration recordings. The results show that the first-mode frequencies are generally in the range between approximately 2.5 Hz and 3.8 Hz, while the second modes are mostly identified between about 3.5 Hz and 5.0 Hz. Where a third mode is consistently detected, its frequency typically lies between roughly 4.2 Hz and 7.5 Hz.

Table 4. Summary of identified natural frequencies and statistical variability for the monitored viaducts in the year 2023.

Viaduct	Mode	Mean	Std	CoV
2A2	1	3.74	0.051	1.36%
	2	3.97	0.035	0.88%
	3	4.17	0.045	1.08%
2B4	1	2.59	0.071	2.73%
	2	4.96	0.088	1.78%
	3	6.02	0.031	0.53%
210	1	3.73	0.096	2.58%
	2	4.33	0.096	2.21%
223	1	3.71	0.052	1.41%
	2	4.35	0.075	1.72%
	3	7.52	0.140	1.87%
233	1	3.02	0.033	1.11%
	2	3.55	0.043	1.22%
	3	2.59	0.036	1.37%
243	1	2.46	0.039	1.59%
	2	3.82	0.053	1.39%
	3	4.77	0.036	0.76%

The variability of the identified frequencies is limited for all structures, with CoV values ranging from about 0.5% to 2.7%. Overall, the statistics reported in Table 4 indicate stable and repeatable frequency estimates across the annual monitoring period despite the use of short-duration records.

Table 5 summarizes the mean frequency, standard deviation, and coefficient of variation (CoV) computed for the three identified modes using both approaches (i.e., separated 102.4 s records and merged 102.4 s records) for viaduct 2A2. Similar considerations apply to all other viaducts.

Table 5. Comparison between separated 102.4 s approach and merged 102.4 s approach for viaduct 2A2 in the year 2023.

	Separate 102.4 s Records			Merged 102.4 s Records		
Mode	**Mean**	**Std**	**CoV**	**Mean**	**Std**	**CoV**
1	3.74	0.051	1.36%	3.75	0.045	1.19%
2	3.97	0.035	0.88%	3.95	0.012	0.31%
3	4.17	0.045	1.08%	4.16	0.041	1.00%

The differences between the two methods are minimal: the mean frequencies vary by less than 0.01 Hz, and the CoV values remain below 1.5% for all modes.

The merged dataset yields marginally smaller standard deviations, confirming the statistical consistency of the results but indicating no significant gain in information with respect to the separate analysis of the short-duration records.

The mode shapes associated with each identified mode were obtained by computing the average of all mode shapes belonging to the same cluster.

Figure 16 presents the first three modal shapes identified for the monitored viaduct using the three-set approach.

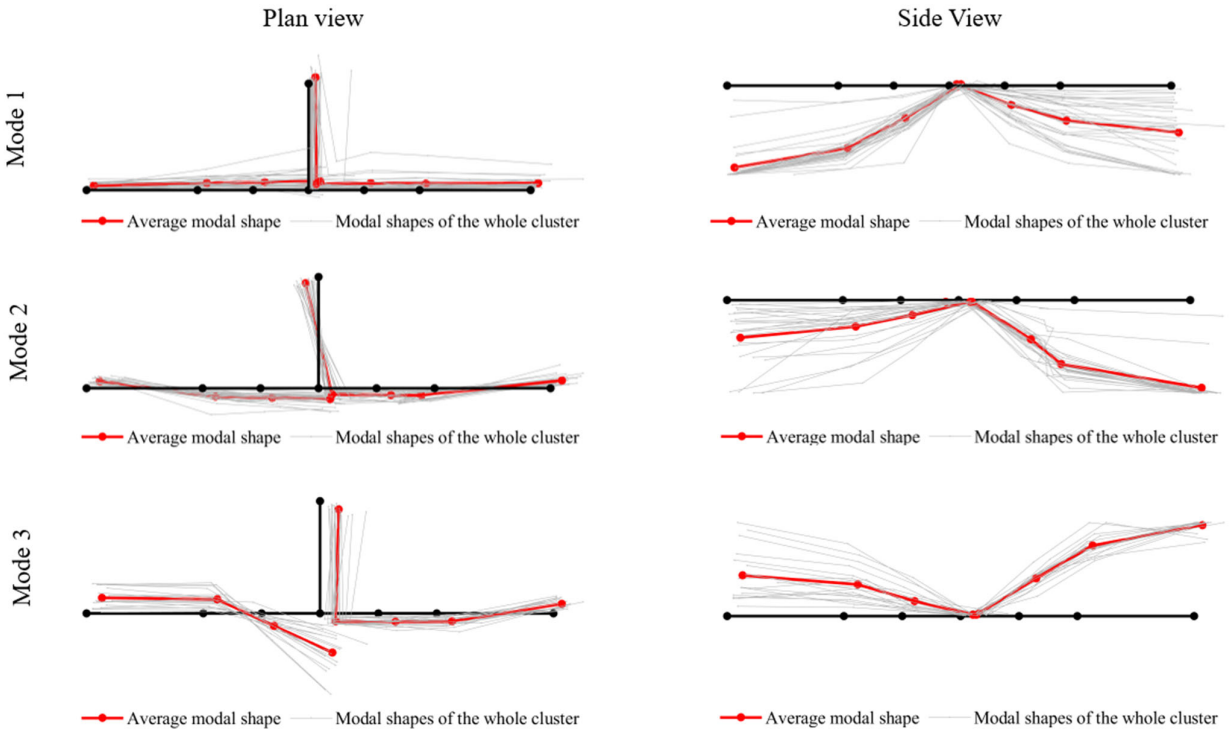

Figure 16. Identified modal shapes for the viaduct 2A2.

All three modes exhibit a predominantly vertical character. However, since the monitoring system was installed only on one of the two longitudinal girders, it is not possible to clearly distinguish whether the detected modes are purely flexural or include a torsional component of the deck.

The horizontal displacements are generally small compared to the vertical ones, particularly for Mode 1 and Mode 2, which display nearly pure vertical motion. In Mode 3, horizontal movements become slightly more pronounced, indicating a modest increase in coupling effects between vertical and lateral responses.

From the plan view, the relative horizontal motion of the two adjacent spans is clearly visible and provides experimental evidence of the decoupled behavior introduced by the support system. Specifically, the suspended span does not follow the motion of the span directly supported on the pier, but exhibits an independent displacement pattern. This confirms the influence of the hanging-link connection, which allows the two spans to vibrate with distinct dynamic characteristics despite their physical continuity.

The procedure described above results in a comprehensive characterization of the dynamic behavior of each monitored structure.

4.6. Analysis of Short Triggered Recordings

In addition to the scheduled 102.4 s acquisitions used for Operational Modal Analysis, the monitoring system also produced short triggered accelerograms of 12.8 s duration (corresponding to 1024 samples per axis), automatically recorded when acceleration thresholds were exceeded. These data provide valuable information on the bridge response to transient or high-intensity events, such as heavy-vehicle passages or sudden dynamic excitations.

Although the primary focus of this study is on the modal identification based on scheduled records, the triggered acquisitions were also systematically processed to evaluate the peak dynamic response of the structure and its temporal evolution.

For each sensor, the peak-to-peak acceleration was computed from every triggered record, and the resulting maxima were aggregated on a monthly basis to identify possible variations or trends in structural behavior over time.

This indicator provides a concise yet effective metric for assessing the evolution of structural response over time.

Figure 17 shows the monthly trend of the maximum peak-to-peak accelerations measured in the vertical (gravitational) direction for all accelerometers installed on the composite viaduct 2A2. The sensors are mounted on the edge girder of span 4 (C4) and span 5 (C5) at three longitudinal positions—L/8, L/4, and L/2—while two additional sensors (P5 N and P5 S) are located on the pier between the spans.

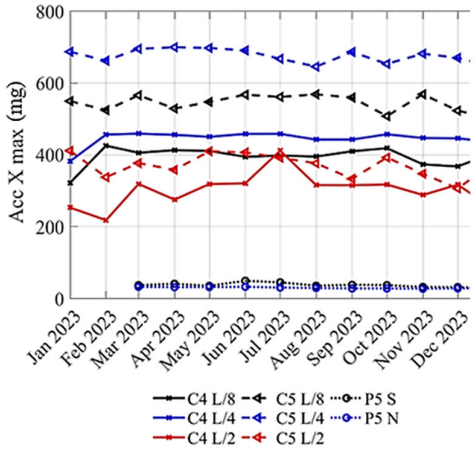

Figure 17. Maximum monthly peak-to-peak accelerations of viaduct 2A2.

The curves indicate that the highest vertical accelerations are consistently observed at L/4 and L/8, whereas the mid-span (L/2) positions exhibit slightly lower amplitudes.

This spatial distribution is consistent with the first vertical bending modes of the deck, where maximum curvature—and therefore higher acceleration—is expected near the quarter-span locations under the predominant traffic-induced excitations acting on the edge girder.

The pier sensors record very low vertical acceleration levels, as expected in regions of constrained vertical motion, confirming the expected boundary behavior of the monitored spans.

Over the monitoring period (January 2023–December 2023), the vertical acceleration levels remain remarkably stable, exhibiting only minor seasonal variations—slightly higher during colder months and lower during summer. These fluctuations are plausibly associated with temperature-dependent stiffness variations in the steel–concrete composite system [38,40]. No progressive drift or sudden changes in acceleration amplitude are observed, suggesting the absence of any significant stiffness loss or structural degradation during the observation period.

Overall, the results confirm a consistent vertical dynamic response across all sensors and throughout time.

The stable acceleration trends obtained from the triggered recordings provide an independent validation of the overall structural performance and complement the modal identification results discussed in Sections 4.4 and 4.5, where the focus shifts to the analysis of scheduled acquisitions for Operational Modal Analysis.

5. Discussion of Results

While the proposed methodology has proven effective in extracting stable and repeatable modal parameters from short-duration acceleration records, several inherent limitations must be acknowledged. These constraints are mainly linked to the short record length and poor sampling frequency. Moreover, the small number of acquisition points (sensors) on each deck influenced the accuracy and robustness of the identification process.

A first limitation concerns the frequency resolution, which is directly proportional to the duration of the recorded signals. For the adopted 102.4 s acquisitions, the spectral resolution is approximately 0.01 Hz, which may not be sufficient to fully resolve closely spaced or interacting modes—a common feature in composite steel–concrete decks [36,37]. This results in some ambiguity in separating adjacent modes, particularly at higher orders or where coupling effects are significant. The comparison between the three-set and merged-signal approaches confirms this behavior: although the merged dataset provides slightly finer frequency sampling, it does not yield appreciably more accurate or stable modal frequencies. Extending the signal length artificially therefore offers only limited benefit for improving resolution.

A second limitation is related to the signal-to-noise ratio of the short recordings. These signals are more sensitive to transient disturbances and operational variability, which can bias the estimation of damping ratios and occasionally generate spurious poles in the stabilization diagrams [41]. The automated signal-selection algorithm mitigates this effect by prioritizing the most energetic recordings, yet some variability in damping estimates remains unavoidable. Moreover, concatenating multiple short recordings does not improve the signal-to-noise ratio; on the contrary, it can introduce non-stationary effects, such as minor phase discontinuities and duplicated poles, caused by different excitation conditions between consecutive acquisitions.

A further source of uncertainty lies in the spectral content of the ambient excitation. The bridges are mainly excited by random traffic loads, which are inherently non-uniform

in frequency and amplitude. Consequently, some vibration modes, especially those weakly excited by operational loads, may not appear consistently in every dataset. This limitation is intrinsic to ambient-vibration testing rather than to the proposed processing method itself [38].

It should be noted that, in long-term OMA applications on bridges in service, the type of excitation strongly influences modal observability. Modes that are excited under purely ambient conditions may become less visible or be masked when traffic-induced excitation dominates specific frequency ranges. For this reason, structural assessment and damage evolution tracking in operational conditions typically rely on modes that are consistently excited under traffic, whereas low-energy modes may provide limited robustness for continuous monitoring.

Finally, the sparse spatial density of sensors affects the completeness and resolution of the identified mode shapes. The limited number of accelerometers, selected for cost-efficiency and ease of installation, restricts the capability to reconstruct higher-order or localized modes. While the main global modes are clearly captured, asymmetric or torsional responses cannot be fully characterized, and the results must therefore be interpreted cautiously.

In summary, these limitations define the boundaries of applicability of short-duration OMA for bridge monitoring. The comparison between the three-set and merged-signal approaches demonstrates that artificially extending the signal duration does not significantly enhance modal identification and may even introduce additional artifacts. Nevertheless, by maximizing the information extracted from limited data, the proposed procedure allows a coarse yet meaningful evaluation of the structural dynamics, which can still provide practical insight for assessing the condition of large bridge systems and for informing future monitoring strategies within digital-twin frameworks. In the proposed case study, the number of sensors was clearly not enough to validate a digital twin, as the available modal information was constrained by the limited sensor density and cannot support a detailed reconstruction of torsional or axial modal shapes.

6. Conclusions

This study presents a critical evaluation of a signal-based methodology for the dynamic identification of composite steel–concrete bridges using short acceleration records. The monitoring system used was extremely simple, composed of only a few wireless accelerometers collecting brief and intermittent recordings of 102.4 s. Although such a configuration is far from ideal for high-resolution Operational Modal Analysis, the work demonstrates that, through careful data selection, filtering, and statistical validation, it is still possible to obtain physically meaningful insights into the structural behavior of the bridge.

The proposed methodology, integrating energy-driven signal selection, SSI-Cov identification, and DBSCAN clustering, is able to identify the main vibration modes of the monitored viaducts. Both the three-set and merged-signal approaches reproduce the dominant modal alignments observed in the full dataset. However, the comparison clearly shows that artificially extending the signal duration by concatenating short recordings does not lead to any improvement in the stability or accuracy of the modal parameters and may even introduce non-stationary effects and numerical artifacts.

The results confirm that, when data are carefully processed, short independent recordings can provide stable estimates of the fundamental frequencies and mode shapes. Nevertheless, the analysis remains inherently coarse. The limited spatial coverage, low sampling frequency, and high variability of ambient excitation prevent a detailed or fully quantitative characterization of the structure. The methodology essentially squeezes all usable information from the dataset, producing a basic yet credible dynamic fingerprint of the bridge.

The frequency resolution of the short records constrains the separation of closely spaced modes, while the variability of the excitation and the modest signal-to-noise ratio affect the damping estimates and the visibility of higher modes. In addition, the reduced sensor layout limits the identification of torsional or localized behaviors. Despite these intrinsic constraints, the study demonstrates that, even under severe data limitations, a minimal monitoring system can yield some useful results when supported by a robust processing workflow. The resulting modal parameters allow a first-level, coarse evaluation of structural performance, sufficient to identify major changes or degradation trends over time.

Author Contributions: Conceptualization, M.F. and G.B.; methodology, M.F. and G.B.; software, M.F. and A.I.; validation, G.B., M.F. and D.M.; formal analysis, M.F. and A.I.; investigation, A.I.; resources, G.B. and D.M.; data curation, M.F. and A.I.; writing—original draft preparation, M.F. and A.I.; writing—review and editing, G.B. and D.M.; visualization, M.F. and G.B.; supervision, G.B. and D.M.; project administration, G.B. and D.M.; funding acquisition, D.M. All authors have read and agreed to the published version of the manuscript.

Funding: This research received no external funding.

Data Availability Statement: The data presented in this study are available on request from the corresponding author.

Conflicts of Interest: The authors declare no conflicts of interest.

References

1. Neves, L.C.; Frangopol, D.M. Condition, safety and cost profiles for deteriorating structures with emphasis on bridges. *Reliab. Eng. Syst. Saf.* **2005**, *89*, 185–198. [CrossRef]
2. Tibaduiza Burgos, D.A.; Gomez Vargas, R.C.; Pedraza, C.; Agis, D.; Pozo, F. Damage Identification in Structural Health Monitoring: A Brief Review from its Implementation to the Use of Data-Driven Applications. *Sensors* **2020**, *20*, 733. [CrossRef] [PubMed]
3. Rainieri, C.; Fabbrocino, G. *Operational Modal Analysis of Civil Engineering Structures*, 1st ed.; Springer: New York, NY, USA, 2014.
4. Zahid, F.B.; Ong, Z.C.; Khoo, S.Y. A review of operational modal analysis techniques for in-service modal identification. *J. Braz. Soc. Mech. Sci. Eng.* **2020**, *42*, 398. [CrossRef]
5. Hasani, H.; Freddi, F. Operational Modal Analysis on Bridges: A Comprehensive Review. *Infrastructures* **2023**, *8*, 172. [CrossRef]
6. Grimmelsman, K.A.; Lindsey, J.D.; Dufour, R.T.; Norris, J.T. Excitation Related Uncertainty in Ambient Vibration Testing of Bridges. In *Model Validation and Uncertainty Quantification*; Conference Proceedings of the Society for Experimental Mechanics Series; River Publishers: New York, NY, USA, 2014; Volume 3.
7. Komarizadehasl, S.; Huguenet, P.; Lozano, F.; Lozano-Galant, J.A.; Turmo, J. Operational and Analytical Modal Analysis of a Bridge Using Low-Cost Wireless Arduino-Based Accelerometers. *Sensors* **2022**, *22*, 9808. [CrossRef]
8. Tomassini, E.; García-Macías, E.; Venanzi, I.; Ubertini, F. ML-Driven Operational Modal Analysis of Road Bridges: Preliminary Results. In Proceedings of the 10th International Operational Modal Analysis Conference (IOMAC 2024), Naples, Italy, 22–24 May 2024; Lecture Notes in Civil Engineering. Springer Nature: Cham, Switzerland, 2024; p. 514.
9. Peeters, B.; De Roeck, G. One-year monitoring of the Z24-Bridge: Environmental effects versus damage events. *Earthq. Eng. Struct. Dyn.* **2001**, *30*, 149–171. [CrossRef]
10. Ni, Y.Q.; Xia, Y.; Liao, W.Y.; Ko, J.M. Technology innovation in developing the structural health monitoring system for Guangzhou New TV Tower. *Struct. Control Health Monit.* **2009**, *16*, 73–98. [CrossRef]
11. Aktan, E.; Bartoli, I.; Glišić, B.; Rainieri, C. Lessons from Bridge Structural Health Monitoring (SHM) and Their Implications for the Development of Cyber-Physical Systems. *Infrastructures* **2024**, *9*, 30. [CrossRef]
12. He, Z.; Li, W.; Salehi, H.; Zhang, H.; Zhou, H.; Jiao, P. Integrated structural health monitoring in bridge engineering. *Autom. Constr.* **2022**, *136*, 104168. [CrossRef]
13. Brighenti, F.; Caspani, V.F.; Costa, G.; Giordano, P.F.; Limongelli, M.P.; Zonta, D. Bridge management systems: A review on current practice in a digitizing world. *Eng. Struct.* **2024**, *321*, 118971. [CrossRef]
14. Zhang, B.; Ren, Y.; He, S.; Gao, Z.; Li, B.; Song, J. A review of methods and applications in structural health monitoring (SHM) for bridges. *Measurement* **2025**, *245*, 116575. [CrossRef]
15. Magalhães, F.; Cunha, Á.; Caetano, E. Online automatic identification of the modal parameters of a long span arch bridge. *Mech. Syst. Signal Process.* **2009**, *23*, 316–329. [CrossRef]

16. Döhler, M.; Mevel, L. Efficient multi-order uncertainty computation for stochastic subspace identification. *Mech. Syst. Signal Process.* **2013**, *38*, 346–366. [CrossRef]
17. Zhu, Z.; Au, S.K.; Brownjohn, J.; Koo, K.Y.; Nagayama, T.; Bassitt, J. Uncertainty quantification of modal properties of Rainbow Bridge from multiple-setup OMA data. *Eng. Struct.* **2025**, *330*, 119901. [CrossRef]
18. Dederichs, A.C.; Øiseth, O. Data Sampling Frequency Impact on Automatic Operational Modal Analysis Application on Long-Span Bridges. *Top. Modal Anal. Parameter Identif.* **2024**, 9. [CrossRef]
19. Faridi, M.A.; Kuncham, E.; Roy, K. Using limited roving sensors to monitor bridge subjected to random traffic load. *J. Civ. Struct. Health Monit.* **2024**, *14*, 693–710. [CrossRef]
20. Reynders, E. System Identification Methods for (Operational) Modal Analysis: Review and Comparison. *Arch. Comput. Methods Eng.* **2012**, *19*, 51–124. [CrossRef]
21. Rainieri, C.; Magalhaes, F.; Ubertini, F. Automated Operational Modal Analysis and Its Applications in Structural Health Monitoring. *Shock. Vib.* **2019**, 5497065. [CrossRef]
22. Fu, S.; Wu, J. Review of Structural Modal Tracking in Operational Modal Analysis: Methods and Applications. *Appl. Sci.* **2025**, *15*, 7201. [CrossRef]
23. Pereira, S.; Magalhães, F.; Gomes, J.P. Modal tracking under large environmental influence. *J. Civ. Struct. Health Monit.* **2022**, *12*, 179–190. [CrossRef]
24. The MathWorks, Inc. *MATLAB*, version 9.14 (R2023a); The MathWorks Inc.: Natick, MA, USA, 2023.
25. Juang, J.N. *Applied System Identification*; PTR Prentice Hall: Englewood Cliffs, NJ, USA, 1994.
26. Ranieri, C.; Fabbrocino, G. Influence of model order and number of block rows on accuracy and precision of modal parameter estimates in stochastic subspace identification. *Int. J. Lifecycle Perform. Eng.* **2014**, *1*, 317–334. [CrossRef]
27. Chopra, A.K. *Dynamics of Structures—Theory and Applications to Earthquake Engineering*, 2nd ed.; Prentice Hall: Upper Saddle River, NJ, USA, 2000.
28. Ewins, D.J. *Modal Testing: Theory, Practice and Application*, 2nd ed.; Research Studies Press Ltd.: Baldock, UK, 2000.
29. Reynders, E.; Houbrechts, J.; De Roeck, G. Fully automated (operational) modal analysis. *Mech. Syst. Signal Process.* **2012**, *29*, 228–250. [CrossRef]
30. He, Y.; Yang, J.P.; Li, Y.F. A three-stage automated modal identification framework for bridge parameters based on frequency uncertainty and density clustering. *Eng. Struct.* **2022**, *255*, 113891. [CrossRef]
31. Mao, J.; Su, X.; Wang, H.; Li, J. Automated Bayesian operational modal analysis of the long-span bridge using machine-learning algorithms. *Eng. Struct.* **2023**, *289*, 116336. [CrossRef]
32. Liu, W.; Yang, N.; Law, S. Automated operational modal analysis with adaptive DBSCAN-based algorithm and its engineering application. *J. Civ. Struct. Health Monit.* **2025**, *15*, 3509–3534. [CrossRef]
33. Civera, M.; Sibille, L.; Zanotti Fragonara, L.; Ceravolo, R. A DBSCAN-based automated operational modal analysis algorithm for bridge monitoring. *Measurement* **2023**, *208*, 112451. [CrossRef]
34. Ester, M.; Kriegel, H.P.; Sander, J.; Xiaowei, X. A density-based algorithm for discovering clusters in large spatial databases with noise. In Proceedings of the Second International Conference on Knowledge Discovery in Databases and Data Mining, Portland, OR, USA, 2–4 August 1996; pp. 226–231.
35. Guo, J.; Wei, G.; Li, X.; Jin, D.; Liu, F. Modal Identification of Structures with Closely Spaced Modes Based on Improved Empirical Wavelet Transform. *J. Vib. Eng. Technol.* **2022**, *10*, 2625–2640. [CrossRef]
36. Jonscher, C.; Liesecke, L.; Penner, N. Influence of system changes on closely spaced modes of a large-scale concrete tower for the application to structural health monitoring. *J. Civ. Struct. Health Monit.* **2023**, *13*, 1043–1060. [CrossRef]
37. Shang, X.-Q.; Huang, T.-L.; He, Y.-B.; Chen, H.-P. Operational Modal Analysis of Civil Engineering Structures with Closely Spaced Modes Based on Improved Hilbert–Huang Transform. *Sensors* **2024**, *24*, 7600. [CrossRef]
38. Bertagnoli, G.; Ferrara, M.; Lucà, F.; Cigada, A. Effect of Environmental Parameters on Structural Health Status Assessment Using OMA Techniques. *Appl. Sci.* **2023**, *13*, 1477. [CrossRef]
39. Qin, M.; Chen, H.; Zheng, R.; He, X.; Ren, S. An Adaptive Operational Modal Analysis under Non-White Noise Excitation Using Hybrid Neural Networks. *Appl. Sci.* **2022**, *12*, 2471. [CrossRef]
40. Poudel, A.; Kim, S.; Cho, B.H.; Kim, J. Temperature Effects on the Natural Frequencies of Composite Girders. *Appl. Sci.* **2024**, *14*, 1175. [CrossRef]
41. Ebbehøj, K.L.; Tatsis, K.; Couturier, P.; Thomsen, J.J.; Chatzi, E. Short-term damping estimation for time-varying vibrating structures in nonstationary operating conditions. *Mech. Syst. Signal Process.* **2023**, *205*, 110851. [CrossRef]